Investigation of a turbulent premixed combustion flame in a backward-facing step combustor; effect of equivalence ratio

Investigation of a turbulent premixed combustion flame in a backward-facing step combustor; effect of equivalence ratio

By:
Medhat A. Nemitallah[a,b], Gaurav Kewlani[a], S. Hong[a], Santosh J. Shanbhogue[a], Mohamed A. Habib[b] and Ahmed F. Ghoniem[a]

[a] Reacting Gas Dynamics Laboratory, Center for Energy and Propulsion Research, Department of Mechanical Engineering, Massachusetts Institute of Technology, 77 Massachusetts Avenue, Cambridge, MA 02139, United States

[b] KACST TIC for CCS, Mechanical Engineering Department, King Fahd University of Petroleum and Minerals, 31261 Dhahran, Saudi Arabia

Abstract

In the present study, large-eddy simulation (*LES*) is utilized to analyze lean-premixed propane-air flame stability in a backward-step combustor over a range of equivalence ratio. The artificially thickened flame approach coupled with a reduced reaction mechanism is incorporated for modeling the turbulence-combustion interactions at small scales. Simulation results are compared to high-speed particle image velocimetry (*PIV*) measurements for validation. The results show that the numerical framework captures different topological flow features effectively and with reasonable accuracy, for stable flame configurations, but some quantitative differences exist. The recirculation zone (*RZ*) is formed of a primary eddy and a secondary eddy and its overall size is significantly impacted by the equivalence ratio. The temperature distribution inside the recirculation zone is highly non-uniform, with much lower values observed close to the backward step and the bottom wall. The mixture distribution inside the RZ is also non-uniform because of mixing with reactants and heat loss to the walls. The flame is stabilized closer to the backward step as the equivalence ratio increases. At lower fuel fractions, the flame lifts off the step starting at equivalence ratio of 0.63 and the lift off distance is increased while the equivalence ratio is lowered.

Keywords: Flame stability; large eddy simulation (*LES*); particle image velocimetry (*PIV*); premixed flame; recirculation zone (*RZ*); step combustor.

Corresponding author/ M.A.Nemitallah, E-Mail: mahmed@mit.edu and medhatahmed@kfupm.edu.sa and Tel: +966-013860-4959.

Abbreviations and Nomenclature

ATF	Artificially thickened flame	*PIV*	Particle image velocimetry
3-D	Three dimensional	*RANS*	Reynolds averaged Navier-Stokes
CC	Catalytic combustion	*RQLF*	rich-burn quick-quench lean-burn flames
DNS	Direct numerical simulation	*RZ*	Recirculation zone
E	Efficiency function	*SE*	Secondary eddy
H	Step height	*SGS*	Sub-grid scale
JL	Jones-Lindstedt	S_L^0	Laminar flame speed
LES	Large-eddy simulation	*TKE*	Turbulent kinetic energy
LPF	Lean premixed flames	δ_L^0	Laminar flame thickness
PE	Primary eddy		

1. Introduction

Most gas turbine combustors used in power plants and jet engines utilize non premixed flames because of their inherent stability under wide ranges of operating conditions. However, diffusion flames result in high temperature spots and, consequently, high levels of nitric oxides, *NOx*, are generated. Public awareness and legislation have led to strict policies for the reduction of the pollutants. Therefore, alternatives such as lean premixed flames (*LPF*) have been proposed and their application is expanding. In this case, the fuel and oxidizer are mixed upstream in order to prevent the formation of stoichiometric zones and, hence, reduce the combustion temperature and, accordingly, reduce the *NOx* emissions. Unfortunately, lean premixed flames are subjected to combustion instabilities [1,2]. Combustion instabilities are resonant phenomena that occur when a positive feedback is established between the acoustic environment and heat release. Resulting pressure fluctuations can reach critical values at which the engine operation can be affected leading to failure [3].

Combustor geometry and the associated flame anchoring mechanism are some of the most important parameters affecting combustion stability. The combustor geometry determines the size and structure of the recirculation zone formed in order to stabilize a flame [4]. Li and Gutmark [5] studied the flame stability with and without center body recess in dump combustor utilizing bluff-body for stabilization. The results showed that the flame is stabilized and the oscillations are reduced when the center body is recessed. Speth and Ghoniem [6] studied the combustion instabilities of a syngas-air premixed flame in a swirl-stabilized combustor over wide ranges of operating parameters. Their results showed strong dependence of the combustion instabilities on the combustor geometry [7,8], operating conditions and fuel compositions. Altay et al. [9] studied the flame-vortex interaction driven combustion dynamics of a premixed flame in a backward-facing step combustor under different fuel compositions and operating conditions. They observed unstable flames at high equivalence ratio, quasi-stable flames at intermediate equivalence ratio, and long stable flame near the lean blow out limit. Hong et al. [10] studied the impact of fuel composition (C_3H_8/H_2) on the structure of the recirculation zone and its role in lean premixed flame anchoring in a backward-facing step combustor. Their results demonstrated a complex coupling between the size and the structure of the recirculation zone and the flame anchoring. Two counter rotating eddies, a primary eddy (PE) and a secondary eddy (SE), were observed in the recirculation zone at relatively low equivalence ratio. Shrinkage of the SE size was observed while increasing the equivalence ratio until this zone completely disappeared. Adding hydrogen to the fuel resulted in higher temperatures and the motion of the flame tip toward the reactor step [10].

Details of the dynamics and phenomenology of near blow off flames were explained by Shanbhogue et al. [11]. They showed that temporally localized extinction, like holes in the flame structure, occurs close to the blow off conditions. The number of holes increases as the conditions of blow off are approached. Kedia and Ghoniem [12] investigated the anchoring mechanism of a laminar premixed flame anchoring close to a heat-conducting bluff-body. They used a fully resolved unsteady two-dimensional simulations coupled with detailed chemical kinetics for methane-air combustion. Their results showed a shear-layer stabilized flame in the vicinity and downstream of the bluff-body, where favorable ignition conditions are established; and a recirculation zone was formed by the combustion products. Altay et al. [13] investigated the effect of the oscillations in the equivalence ratio on the dynamics of combustion of a lean premixed propane-air flame in a backward-facing step combustor. Equivalence ratio oscillations were performed by altering the location of the fuel injector. They reported that flame-vortex interactions are the primary source of the combustion dynamics and the oscillations in the equivalence ratio have secondary effects.

The effects of the enthalpy of reaction and fuel composition on combustion dynamics were examined by Ferguson et al. [14] utilizing two different combustors, laboratory scale and atmospheric pressure combustors. Different fuel blends of natural gas, ethane and propane were considered for the combustion with air. They observed different dynamic response with increased fraction of propane. Fritsche et al. [15] performed an experimental study of thermoacoustic instabilities in a premixed flame on a swirl stabilized combustor under different inlet temperature and air to fuel ratio. The results showed the existence of two stable flames, one is lean and the other is rich, separated by a range of unstable flames. The unstable flames exhibited different shapes, and pressure oscillations. Seo [16] studied the effect of the operating temperature, combustion chamber pressure, and equivalence ratio on combustion dynamics of a lean-premixed flame on single-element swirl injector using gaseous fuel. Unstable flames were recorded when the equivalence ratio was in the range between 0.5 and 0.7. Also, unstable flames appeared when the inlet temperature was greater than 650 K. Venkataraman et al. [17] studied the effects of inlet Reynolds numbers, swirl number, and equivalence ratio on combustion instabilities of a premixed natural gas-air flame in a coaxial dump combustor stabilized using a bluff-body. Unstable flames were recorded near the lean blowout limit and close to stoichiometric conditions. Combustion stability was affected negatively when the inlet velocity was raised.

In all of these studies, the flame stability, or potential for becoming unstable, was shown to depend on the equivalence ration. In the present study, LES is used to predict the impact of the equivalence ratio on combustion in a rearward facing step combustor. Wide range of equivalence ratios from lean to near stoichiometric is investigated. High resolution, high speed particle image velocimetry (*PIV*) is used to validate the numerical results. The present work focuses on predicting the location of the flame and the structure of the recirculation zone since they contribute significantly to overall combustion dynamics.

2. Combustor set up and PIV system

A planner combustor in which a premixed flame is stabilized near a backward-facing step was used in the experimental work and the simulations. Figure 1 (a) shows a schematic representation of this step combustor and the relevant dimensions. The inlet section of the combustor consists of a rectangular cross section stainless steel duct of a 160 mm span wise width and 40 mm height. Air is fed to the combustor inlet by an Atlas-Copco-GA-30-FF air compressor through a flow meter. The inflow is choked. At an axial location of 0.45 m downstream the choke plate, the cross section of the duct is contracted gradually to a height of 20 mm over an axial distance of 0.15 m, followed by a 0.4 m long and 20 mm height duct of constant cross section area. This is followed by the backward facing step where the height expands with an expansion ratio of 2:1 back to 40 mm. This acts as the nominal anchoring point for the flame. The fuel flow rate is measured using a Sierra C100M mass flow controller before its injection, 20 mm downstream of the choke plate, through a number of holes in the manifold. The mass flow controller allows a maximum flow rate of 2.36 g/s for propane with uncertainty in the measurement of ±1% of the full scale. The distance between the fuel injection point and the backward step is enough to mix the gases very well (see Altay et al. [9]). The length of the combustor downstream the step is 0.5 m and the combustor is opened to the atmosphere. The combustor length is sufficiently short to prevent the coupling with the acoustics (see Hong et al. [10]). The temperature of the air-fuel mixture is measured using a K-type thermocouple located at a distance of 0.2m upstream of the step. In order to allow for optical access to the flame, a quartz window is installed just downstream of the step.

Figure 1-b shows a schematic representation of the particle image velocimetry (*PIV*) system used to measure the 2D velocity fields. The system consists of a *Nd:YLF* laser light source of 527 mm wavelength. The system is equipped with a *NAC GX-1 CMOS* high-speed camera having 1280 ×1024 pixel for imaging at a rate of 1 *kHz*. Spherical and cylindrical lenses with different focal lengths were used in order to generate a light sheet with a thickness of 1 mm. *AL2O3* seeding particles having diameters in the range of 1.5 to 3 μm were injected in the main air flow downstream of the choke plate. The measurements of the *PIV* system were post-processed using the *LaVision DaVis* 7.2 software.

3. LES model

Three approaches are normally considered for the numerical modeling and simulation of turbulent flow and combustion. These approaches are direct numerical simulation (*DNS*), Reynolds averaged Navier-Stokes (*RANS*), and large eddy simulation (*LES*). In the *DNS* model, the entire spectrum of turbulence scales is resolved, from the device to the Kolmogorov scales. This necessitates the use of a very fine mesh and very small time step with a prohibitive large number of mesh points. Consequently, this approach is impractical for engineering applications. At the opposite extreme, *RANS* models solve the time and spatially averaged governing equations, resolving only the large scales while modeling the turbulent fluctuations and their impact on combustion across the scales. This makes it is the least expensive model in terms of the computational time, but with least universality. *LES* approaches lie between these two extremes, in terms of accuracy and the required computational resources. In *LES* models, the governing equations are filtered at a scale smaller than that of the large eddies, which have significant impact on the flow by virtue of their energy. The impact of scales below the filter scales (which, if the filter scale is sufficiently close to the Kolmogorov scale, are expected to behave in a universally predictable way) are modeled using sub-filter scale models. In this work, we apply LES models, examine their accuracy by comparing the predicted results to data of the experimental measurement, and analyze the simulation results.

3.1 Conservation equations

Turbulence transfers energy from the large to the small eddies (cascade) all the way down to the Kolmogorov eddies where energy is dissipated according to the following spectrum [18]:

$$E(k) = C_k \varepsilon^{2/3} k^{-5/3} \quad (1)$$

Where, C_k is the Kolmogorov constant. In LES, the various flow quantities, Φ, are filtered in the spectral space (by suppressing the components greater than a given cut-off length), or in the physical space (weighted averaging in a given volume). The filtered quantity Φ is expressed as follows:

$$\overline{\Phi}(x) = \int \Phi(x')g(x-x')dx' \quad (2)$$

Where, g is a filter function. For variable density flows, like in the present study, Favre, or density-weighted, filtered quantity, Φ, can be expressed as follows:

$$\overline{\rho}\overline{\Phi}(x) = \overline{\rho\Phi} \quad (3)$$

Often, the grid is used as the spatial filter. The conservations equations for the *LES* model can be obtained after filtering each term in mass, momentum, energy, and species transport equations using the Favre filtering operation as follows [18]:

Mass equation:

$$\frac{\partial\bar{\rho}}{\partial t}+\frac{\partial(\bar{\rho}\tilde{u}_j)}{\partial x_j}=0 \tag{4}$$

Where, $\tilde{u}$ is the filtered velocity vector.

Momentum equation:

$$\frac{\partial\bar{\rho}\tilde{u}_i}{\partial t}+\frac{\partial(\bar{\rho}\tilde{u}_j\tilde{u}_i)}{\partial x_j}=\frac{\partial\bar{P}}{\partial x_i}+\frac{\partial\bar{\sigma}_{ji}}{\partial x_j}+\frac{\partial\tau_{ujui}}{\partial x_j} \tag{5}$$

Where, σ is the filtered viscous stress tensor and τ is the corresponding sub-grid scale (*SGS*) term which can be defined as [19]:

$$\tau_{ij}\equiv\rho\overline{u_i u_j}-\rho\bar{u}_i\bar{u}_j \tag{6}$$

The sub-grid-scale stresses resulting from the filtering operation are unknown, and require modeling. This term can be modeled using different approaches like the Smagorinsky approach [20].

Energy equation:

$$\frac{\partial\bar{\rho}\tilde{E}}{\partial t}+\frac{\partial(\bar{\rho}\tilde{u}_j\tilde{E}+\tilde{u}_j\bar{P})}{\partial x_j}=\frac{\partial\bar{q}_j}{\partial x_j}+\frac{\partial\overline{\sigma_{jk}u_k}}{\partial x_j}+\frac{\gamma R}{\gamma-1}\frac{\partial\tau_{uj}T}{\partial x_j}+\frac{\partial\tau_{ujuk}u_k}{\partial x_j} \tag{7}$$

Where, $\tilde{E}$ and $\bar{q}$ are the filtered total specific energy and the filtered heat flux, respectively.

Species transport equation:

$$\frac{\partial\bar{\rho}\tilde{Y}_k}{\partial t}+\frac{\partial(\bar{\rho}\tilde{u}_j\tilde{Y}_k)}{\partial x_j}=\frac{\partial}{\partial x_j}\left(\bar{\rho}D_k\frac{\partial\tilde{Y}_k}{\partial x_j}\right)-\frac{\partial}{\partial x_j}\left[\bar{\rho}(Y_k u_j-\tilde{Y}_k\tilde{u}_j)\right]+\bar{\dot{w}}_k \tag{8}$$

Where, $\tilde{Y}_k$ is the species mass fraction, D is the molecular diffusivity, and $\bar{\dot{w}}_k$ is the reaction rate.

3.2 Combustion modeling technique

For combustion in a turbulent environment, under most conditions, the chemical reactions are confined to thin layers at scales smaller than those resolved on the *LES* grid. In *RANS* models, the averaged chemical source term in the governing equations is modeled in terns of the mean field variables and the modeled fluctuations. In *LES* models, although finer grid resolution is used and some of the large scales are resolved, the instantaneous flame thickness is still too small to be captured by the *LES* grid. In the case of premixed combustion, several approached have been suggested for modeling the filtered reaction rate terms [21]. In the present work, we are interested in models that incorporate finite rate chemistry such as the artificially thickened flame approach which is described briefly below.

3.2.1 Artificially thickened flame model

While maintaining laminar flame speed, the thickened flame approach considers artificially thickening the flame front such that is can be resolved on the *LES* mesh. It is well established from the laminar flame theory for premixed combustion that the laminar flame speed (S_L^0), molecular diffusivity (D), laminar flame thickness (δ_L^0), and the mean reaction rate ($\overline{\dot{w}}_k$) can be related as follows:

$$S_L^0 \propto \sqrt{D\overline{w}},\ \delta_L^0 \propto D / S_L^0 = \sqrt{D/\overline{w}} \tag{9}$$

From this relation, the flame thickness can be increased by a factor F while maintaining the same laminar flame speed. This can be done through the modification of the molecular diffusivity to FD and the reaction rate to $\overline{\dot{w}}_i/F$. Thus, the modified expressions become:

$$\overline{S_L^0} \propto \sqrt{FD\frac{\overline{w}}{F}} = S_L^0,\ \overline{\delta_L^0} \propto FD / \overline{S_L^0} = F\,\delta_L^0 \tag{10}$$

If F is sufficiently large, the thickened flame front can be resolved on the LES computational grid. Based on the above discussion, the filtered species transport equation can be expressed as follows:

$$\frac{\partial\overline{\rho}\widetilde{Y}_i}{\partial t} + \frac{\partial(\overline{\rho}\widetilde{Y}_i\widetilde{u}_j)}{\partial x_j} = \frac{\partial}{\partial x_j}\left(\overline{\rho}FD_i\frac{\partial\widetilde{Y}}{\partial x_j}\right) + \frac{\overline{\dot{w}}_k}{F} \tag{11}$$

Changing the flame front thickness results in modifications in the turbulence-chemistry interaction. The flame becomes less sensitive to the turbulence and the flame front wrinkling is also reduced. To recover some of these interactions, an efficiency function (E) has been incorporated and the filtered equation for the species transport becomes [22]:

$$\frac{\partial\overline{\rho}\widetilde{Y}_i}{\partial t} + \frac{\partial(\overline{\rho}\widetilde{Y}_i\widetilde{u}_j)}{\partial x_j} = \frac{\partial}{\partial x_j}\left(\overline{\rho}EFD_i\frac{\partial\widetilde{Y}}{\partial x_j}\right) + \frac{E\overline{\dot{w}}_k}{F} \tag{12}$$

A dynamic formulation has been incorporated to model the efficiency function. In this formulation, the thickening factor and the diffusivity are represented locally as follows [23]:

$$F_{loc} = 1 + (F-1)\Psi(c) \tag{13}$$

And:

$$D_{i,loc} = \frac{\mu}{Sc}EF_{loc} + (1-\Psi(c))\frac{\mu_t}{Sc_t} \tag{14}$$

Where, $\Psi(c)$ is a locally defined sensor function based on the reaction progress variable, c, which can be expressed as follows:

$$\Psi(c) = 16[c(1-c)]^2 \tag{15}$$

And:

$$c = 1 - \frac{Y_F}{Y_F^{in}} \tag{16}$$

Where, Y_F is the fuel mass fraction in the cell and Y_F^{in} is the fuel mass fraction at inlet. Sc is the Schmidt number, μ is the dynamic viscosity, and F_{loc} and D_{loc} are the local thickening factor and the local diffusivity, respectively. Based on that, the filtered species transport equation can be expressed as follows:

$$\frac{\partial\overline{\rho}\widetilde{Y}_i}{\partial t} + \frac{\partial(\overline{\rho}\widetilde{Y}_i\widetilde{u}_j)}{\partial x_j} = \frac{\partial}{\partial x_j}\left(\overline{\rho}EF_{loc}D_{i,loc}\frac{\partial\widetilde{Y}}{\partial x_j}\right) + \frac{E\overline{\dot{w}}_k}{F_{loc}} \tag{17}$$

Various models were presented to define the function E in terms of a dimensionless wrinkling factor (the ratio of flame surface to its projection in the direction of its propagation). In the present work, the models suggested by Colin [22] and Charlette [24,25] have been incorporated. *OpenFOAM* has been used to perform the simulations.

3.2.2 Reaction kinetics mechanism

The artificially thickened flame (*ATF*) approach allows for finite rate kinetics as described by Arrhenius rate laws to be used in the calculations, as in the case of *DNS* model. Global single step reaction kinetics cannot capture some of the flame characteristics especially at conditions in which the premixed flames interact strongly with flow gradients. However, the reaction mechanisms should have a small number of reaction steps with fewer intermediate species to limit the computation complexity [26]. In this study, the multi-step reaction mechanism by Jones-Lindstedt (*JL* mechanism) [27] for propane-air combustion has been incorporated. The parameters of the JL mechanism (listed in Table 1) have been coded in the *CHEMKIN* format and coupled to the *OpenFOAM* software.

4. Operating and boundary conditions

The backward-facing step combustor geometry is shown in Fig.1-c. The combustor has an inlet channel height (*H*) of 20 mm upstream of the step and a channel height of 40 mm downstream of the step. Upstream of the step, the inlet channel length is 50 mm which is long enough to allow for further flow development before reaching the step. The total length of the combustor channel downstream of the step is 350 mm with a fixed width of 160 mm.

A parallelized, unstructured, finite volume *LES* code was used for solving the reactive compressible *3-D* Navier-Stokes equations with second-order spatial and temporal accuracy. The one-equation eddy viscosity model was employed to estimate the sub-grid scale (*SGS*) stress terms. The choice of the numerical grid was controlled by the values of the physical length scales of the flow. Pope [28] suggested a filter-width (Δ) to integral length scale (L_I) ratio of 0.083 in order to resolve at least 80% of the turbulent kinetic energy and capture the bulk of the energy containing structures. Using the step height (*H*) as the integral length scale, the filter-width was estimated to be 1.8 mm. Based on that, a non-uniform mesh was created using *OpenFOAM* consisting of approximately 16,600 cells in the x-y plane. Downstream the step, the total number of cells in the x and y directions are 270 and 59, respectively. The corresponding values of grid size in the x and y directions, Δx and Δy, are 1.0 mm and 0.5 mm, respectively. In order to prevent excessive numerical dissipation or instability, the temporal resolution was determined based on physical time scale estimates as function of velocity and grid size. The time step for the simulations was estimated at approximately 2.8 μs; however, a value of 1 μs was used in order to adequately resolve the chemical time scales and consider local refinement and acceleration of the fluid above the bulk inlet velocity.

In all simulations, the inlet velocity was fixed to 5.2 m/s, which corresponded to a fixed Reynolds number of 6,500. The inlet flow temperature was kept unchanged at 293 K. The effects of the equivalence ratio on the size of the recirculation zone and flame stability were numerically investigated over the range of 0.45 to 0.85. Details of the experimental study were reported in Hong et al. [10]. All simulations were performed in *3D* while considering periodic boundary conditions in the z-direction, and at atmospheric pressure. Inlet uniform velocity with fluctuations of around 5% of the inlet average value was considered in all simulations in order to model turbulence in the incoming flow. To initiate the flame, a high temperature pulse was applied just before the combustor step to ignite the fuel. Thus the reacting mixture is convected downstream and eventually stabilizes the flame in the wake of the step. The no-slip conditions were applied along all walls while the zero Neumann condition was specified for the other variables. At the exit section of the reactor, zero Neumann conditions were specified for all variables except the pressure, for which wave-transmissive conditions were used. To resolve the flow features in the wall boundary layer and to maintain reasonable computational efficiency, appropriate wall functions were utilized. Heat transfer was considered at the walls to account for heat losses. Numerical computations started with quiescent conditions and the unsteady flow characteristics evolve naturally, and the total computation time was set to 0.3 *s* in all simulations.

5. Results and discussions

The results of the experimental and numerical investigation are presented in this section. These results include the recirculation zone shape and structure in addition to the flame location and overall shape (macrostructure). The numerical results obtained using the present *LES* model are compared with the corresponding PIV measurements under different conditions. The impact of equivalence ratio on the flow field and flame stabilization is also examined.

5.1 Model validation and the flow-field

Figure 2 depicts a comparison of the numerical results for both of the average and the *rms* of the axial velocities at an equivalence ratio of 0.63 with the *PIV* measurements. The plots are presented on a background of the streamlines of the mean flow velocity in order to highlight the important flow features such as the recirculation zones. The mean axial velocity is first reduced because of the expansion over the step, followed by the formation of recirculation zone due to unfavorable pressure gradient. The velocity increases within the shear layer and downstream of the recirculation zone as a result of combustion heat release. The axial *rms* velocity values are highest within the shear layer. This can be attributed to the growth of local instability within the shear layer and to the roll-up of coherent vortices. Small reduction in the turbulence intensity is observed within the mixing layer due to the heat release from the combustion process. Good agreement between the experimental measurements and the corresponding numerical results can be seen in the figure in terms of the overall features and average and *rms* axial velocity contours. The overall length of the recirculation zone, primarily impacting the size of the secondary eddy, is under-predicted.

As can be seen from Fig.2, there are two eddies inside the recirculation zone at the equivalence ratio of 0.63. The first is the large primary eddy (*PE*) spinning in the clockwise direction and constituting most of the recirculation zone. The second is the secondary eddy (*SE*) spinning in the opposite direction and located between the step and the PE close to the corner. The sizes of both *PE* and *S*E are controlled by the equivalence ratio. For more detailed presentations of the *LES* model results and the *PIV* data at the equivalence ratio of 0.63, Figs. 3 and 4 present line plots of the normalized axial average and *rms* velocities at different axial locations. The predicted flow evolves faster than the measurements since, as mentioned above; the size of SE is under predicted. The plots indicate overall good agreement between the *LES* model and the experimental data. Because of the heat release from the combustion process and turbulent dilatation, the flow field is modified and the axial average velocity is increased downstream. The turbulence intensity is high in the region close to the upper wall and in the shear layer area where flow separation and shear layer instability lead to vortex shedding and associated fluctuations. As shown in Fig.4, the velocity fluctuation is under-predicted in the upper half of the combustor. This may be attributed to several reasons such as the use of periodic boundary conditions and how the inlet fluctuations are modeled. Close to the reattachment zone (*x/H*>5), the streamlines curvatures are the highest. Significant unsteadiness is typically experienced by the flow around the reattachment point. As a result, the velocity fluctuations and the turbulent kinetic energy (*TKE*) increase.

Figure 5 shows the contours of the average axial velocity at different equivalence ratios based on the *PIV* measurements. Streamlines-based arrows depict the direction of the flow and the colors shown in the color bars illustrate the mean velocity field. As the equivalence ratio is raised, the size of the PE is reduced and its location is displaced upstream toward the step. The *SE* size is also reduced with increasing the equivalence ratio and it is almost collapsed at equivalence ratio of 0.85 as shown in Fig.5-c. The higher temperature ratio across the flame leads to faster acceleration of the flow and the reduction of the overall recirculation zone length. These findings show the strong dependence of the flow field and recirculation zone on the equivalence ratio in premixed combustion.

5.2 The reactive field

Figure 6 depicts the temperature contours at different equivalence ratios based on the LES results. The results are obtained at fixed inlet Reynolds number for a range of equivalence ratio of 0.5 and 0.85. As shown in the figure, the flame tip or leading edge moves toward the step as the equivalence ratio increases. At lower equivalence ratios, the flame is stabilized in the vicinity of the middle of the average recirculation zone (further away form the step) where it is ignited by the recirculating products. This is supported by experimental data; see Hong et al. [29]. At higher equivalence ratios, the size of the recirculation zone is reduced, the temperature levels are increased and the flame is moved to upstream locations. The flame tip propagates upstream with respect to the recirculation zone, anchoring at the near the step where the primary eddy forms. The angle of the flame with respect to the flow also increases at higher equivalence ratios, consistent with the higher burning velocity of the embedded laminar flames. It is clear that the flame is able to move further into the reactants stream and upstream towards the step. It is also interesting to see that the temperature of the recirculating gases near the step remains significantly lower than that of the products downstream of the flame.

Mixing with reactants and heat loss to the walls near the step contributes to the temperature distribution within the recirculation zone. This feature must be considered when modeling flame stabilization in confined domains. Experimental results supporting these trends were reported in Hong et al. [10,29]. The reduction in temperature in this region is partly due to the entrainment of the reactants into the recirculation zone and partly due to its proximity to the step and channel walls. The temperature in the secondary eddy is the lowest at the lower equivalence ratio where the flame is anchored a significant distance away from the step, thus, making it possible for reactants to diffuse across the layer near the step. It is also interesting to see that, at low equivalence ratios, the flame is stabilized/embedded within the shear layer where significant waviness is exhibited. On the other hand, the flame propagates outwards and further into the reactants stream at higher values of the equivalence ratio. As the flame propagates outwards with respect to the shear layer and towards the reactants, its angle increases and it anchors closer to the step. Less reactant survives and the temperature in the RZ increases.

The profiles of temperature and species concentrations are presented in Fig.7 at different axial locations within and across the recirculation zone at equivalence ratio of 0.85. The temperature is low in the upper part of the combustor corresponding to the incoming cold flow, and is high in the lower part because of the presence of the flame and the recirculating hot products. Close to the lower wall, the temperature is the lowest especially close to the step because of the heat loss to the walls and mixing with the reactants. The temperature profiles show the flame spreading along the shear layer. The CO_2 profiles show areas filled with products but cooled by their proximity to the walls. Further downstream, the flame approaches the upper wall. On the other hand, the upper wall temperature remains close to the inlet temperature. Because of convective heat loss, oxygen concentrations are highest in the incoming stream and they are reduced in the lower half due to consumption and dilution by the products. The low oxygen concentration spreads into the upper half of the combustor as the flame spreads upward.

An interesting observation is the presence of relatively high concentration of oxygen in the upstream portions of the recirculation zone, x/H=0.25, significantly higher than that found in the downstream regions. While finite oxygen concentrations should be expected since the mixture is lean, the higher values closer to the step indicate that reactants are transported across the shear layer and remained unburned, especially at lower values of the equivalence ratio. Note that O_2 concentration decreases within the shear later where reactions are active and increases towards the lower wall. The concentrations of carbon dioxide (CO_2) resemble the temperature concentrations since CO_2 is one of the primary combustion products, except close to the walls where the temperature decreases because of heat loss. Similar to the temperature, average values of CO_2 reached a maximum within the mixing layer. The concentrations of intermediate species, CO and H_2, are highest in the region in the vicinity of the step and they are reduced in the axial direction due to their oxidation to CO_2 and H_2O, respectively. Nevertheless, finite concentrations of intermediates, especially CO, persist untill the exit.

Figure 8 shows the effect of the equivalence ratio on the temperature distribution along the combustor. The figure presents the axial distribution of the instantaneous temperature along the line y/H=0, the lower and upper walls average temperatures and the axial mean velocity along the line y/H=0. As the equivalence ratio is raised, the burning velocity and products temperature is increased, and the flame front is propagated upstream and upward into the reactants stream. Both the products temperature and the proximity of the flame and products to the lower walls raise its temperature as the equivalence ratio increases from 0.45 to 0.85, as shown in Figs.8-b and 8-c. Fig.8-a shows clear distinction between the flame shape and position at lower and higher equivalence ratios. At lower values, Fig.8-a, the flame is initiated downstream (the flame "lifts off" the step) and stabilizes in the region of low velocity inside the recirculation zone. This is clear from the temperature and species concentrations shown in Figs. 6 and 7. Further reduction in the equivalence ratio results in longer flame lift off distance. Simulations show that the flame blows out at equivalence ratio of around 0.45. The temperature distribution confirms that the flame tip moves upstream as the equivalence ratio is raised. At intermediate values, the flame is anchored close to the step. Due to the higher density ratio across the flame at higher fuel concentration in the reactants, and the associated volumetric expansion in the products, the average axial velocity grows in the axial direction as presented in Fig.8-d.

6. Conclusions

Results of a large eddy simulation of premixed combustion in a rearward facing step combustor were presented under lean to close-to-stoichiometric conditions. The flame is stabilized close to the step at a distance that decreases as the equivalence ratio increases. The artificially thickened flame method along with a multi-step reaction mechanism is used in *OpenFOAM*. The numerical results for the flow field characterization were compared with experimental data of high-speed particle image velocimetry (*PIV*). Results showed that the numerical solution is able predict the flow with reasonable agreement, although some quantitative differences exist. Two eddies, the primary eddy (*PE*) rotating in the clockwise direction and the secondary eddy (*SE*) rotating in the opposite direction, appear inside the recirculation zone. The SE nearly disappears at higher (but lean) equivalence ratios. The equivalence ratio significantly affects the flow field. At lower equivalence ratio, the flame is initiated downstream (flame lift-off) and stabilizes in the region of low velocity inside the recirculation zone close to the reattachment point. At higher values of equivalence ratios, the flame approaches the step and penetrates deeper into the reactants. The recirculation zone temperature is significantly below that of the products because of mixing with the reactants and the heat loss to the boundaries. At lower fuel fractions, the flame is embedded in the shear layer while at higher values, it propagate outwards into the reactants stream.

Acknowledgement

The support of King Fahd University of Petroleum and Minerals through KFUPM-MIT Research Collaboration Center through grant number R12-CE-10 to carry out this investigation is highly acknowledged.

References:

[1] Altay HM, Hudgins DE, Speth RL, Annaswamy AM, Ghoniem AF. Mitigation of thermoacoustic instability utilizing steady air injection near the flame anchoring zone. Combustion and flame 2010;157:686-700.

[2] Ghoniem AF, Park S, Wachsman A, Annaswamy A, Wee D, Altay HM. Mechanism of combustion dynamics in a backward-facing step stabilized premixed flame. Proceedings of the combustion institute 2005;30:1783-1790.

[3] Lee K, Kim H, Park P, Yang S, Ko Y. CO_2 radiation heat loss effects on NOx emissions and combustion instabilities in lean premixed flames. Fuel 2013;106:682-689.

[4] Yadav NP, Kushari A. Visualization of recirculation in low aspect ratio dump combustor. Journal of flow visual image process 2009;16:127-136.

[5] Li G, Gutmark EJ. Effect of nozzle geometry on combustion flow field and combustion characteristics. Proceedings of the combustion institute 2005;30:2893-2901.

[6] Speth RL, Ghoniem AF. Using a strained flame model to collapse dynamic mode data in a swirl-stabilized syngas combustor. Proceedings of the combustion institute 2009;32:2993-3000.

[7] Speth RL, Hong S, Shanbhogue SJ, Ghoniem AF. Mode selection in ame-vortex driven combustion instabilities. 49th AIAA aerospace sciences meeting 2011;236.

[8] Speth RL. Fundamental studies in hydrogen-rich combustion: in- stability mechanisms and dynamic mode selection. PhD thesis, Massachusetts Institute of Technology 2010.

[9] Altay HM, Speth RL, Hudgins DE, Ghoniem AF. Flame-vortex interaction driven combustion dynamics in a backward-facing step combustor. Combustion and flame 2009;156:1111-1125.

[10] Hong S, Shanbhogue SJ, Ghoniem AF. Impact of fuel composition on the recirculation zone structure and its role in lean premixed flame anchoring. 35th International symposium on combustion, San Francisco-USA 2014.

[11] Shanbhogue SJ, Husain S, Lieuwen T. Lean blow-off of bluff body stabilized flames: scaling and dynamics. Progress in energy and combustion science 2009;35:98-120.

[12] Kedia KS, Ghoniem AF. The anchoring mechanism of a bluff-body stabilized laminar premixed flame. Combustion and flame 2014;161:2327-2339.

[13] Altay HM, Speth RL, Hudgins DE, Ghoniem AF. The impact of equivalence ratio oscillations on combustion dynamics in a backward-facing step combustor. Combustion and flame 2009;156:2106-2116.
[14] Ferguson D, Straub D, Richards G, Robey E. Impact of fuel variability on dynamic instabilities in gas turbine combustion. 5th US combustion meeting 2007.
[15] Fritsche D, Furi M, Boulouchos K. An experimental investigation of thermoacoustic instabilities in a premixed swirl-stabilized flame. Combustion and flame 2007;151:29-36.
[16] Seo S. Parametric study of lean-premixed combustion instability in a pressurized model gas turbine combustor. Ph.D. thesis 1999; Department of mechanical and nuclear engineering, the Pennsylvania state University: University Park, PA.
[17] Venkataraman KK, Preston LH, Simons DW, Lee BJ, Lee JG, Santavicca DA. Mechanisms of combustion instability in a lean premixed dump combustor. Journal of propulsion and power 1999;15:909-918.
[18] Perez FEH. Sub-filter scale modeling for large eddy simulation of lean hydrogen-enriched turbulent premixed combustion. Ph.D. thesis 2011: University of Toronto.
[19] Hinze JO. Turbulence. McGraw-Hill Publishing Co. 1975; New York.
[20] Smagorinsky J. General circulation experiments with the primitive equations: I. the basic experiment. Month weather review 1963;164:91-99.
[21] Echekki T. Turbulent combustion modeling: advances, new trends and perspectives. Springer-verlag 2011.
[22] Colin O, Ducros F, Veynante D, Poinsot T. A thickened flame model for large eddy simulation of turbulent premixed combustion. Physics of fluids 2000;12:1843-1863.
[23] Durand L, Polifke W. Implementation of the thickened flame model for large eddy simulation of turbulent premixed combustion in a commercial solver. ASME Paper 2007; No. GT2007-28188.
[24] Charlette F, Meneveau C, Veynante D. A power-law flame wrinkling model for LES of premixed turbulent combustion Part I: non-dynamic formulation and initial tests. Combustion and flame 2002;131:159-180.
[25] Charlette F, Meneveau C, Veynante D. A power-law flame wrinkling model for LES of premixed turbulent combustion Part II: dynamic formulation. Combustion and flame 2002;131:181-197.
[26] Roux S, Lartigue G, Poinsot T, Meier U, Berat C. Studies of mean and unsteady flow in a swirled combustor using experiments, acoustic analysis, and large eddy simulations. Combustion and flame 2005;141:40-54.
[27] Jones WP, Lindstedt RP. Global reaction schemes for hydrocarbon combustion. Combustion and flame 1998;73:233-249.
[28] Pope SB. Turbulent flows. Cambridge University Press 2000.
[29] Hong S, Speth RL, Shanbhogue SJ, Ghoniem AF. Examining flow-flame interaction and the characteristic stretch rate in vortex-driven combustion dynamics using PIV and numerical simulation. Combustion and flame 2013;160:1381-1397.

Table 1 Propane-air reaction kinetics mechanism [27].

Jones-Lindstedt (CHEMKIN format)	*A* (pre-exponential coefficient)	β (Temperature exponent)	*Ea* (activation energy)
C_3H_8 + 1.5 O_2 => 3CO+ 4H_2	7.1E+13	0.00	3.0E+4
FORD /C_3H_8 0.5/ FORD /O_2 1.25/			
C_3H_8 + 3H_2O => 3CO + 7H_2	3.0E+11	0.00	3.0E+4
H_2 + 0.5 O_2 => H_2O	1.21E+18	-1.0	4.0E+4
FORD /H_2 0.25/ FORD /O_2 1.5/			
H_2O + 0 O_2 +0 H_2 => H_2 + 0.5 O_2	7.06E+17	-0.877	9.8E+4
FORD /H_2 -0.75/ FORD /O_2 1/ FORD /H_2O 1/			
CO + H_2O = CO_2+H_2	2.75E+12	0.00	2.0E+4

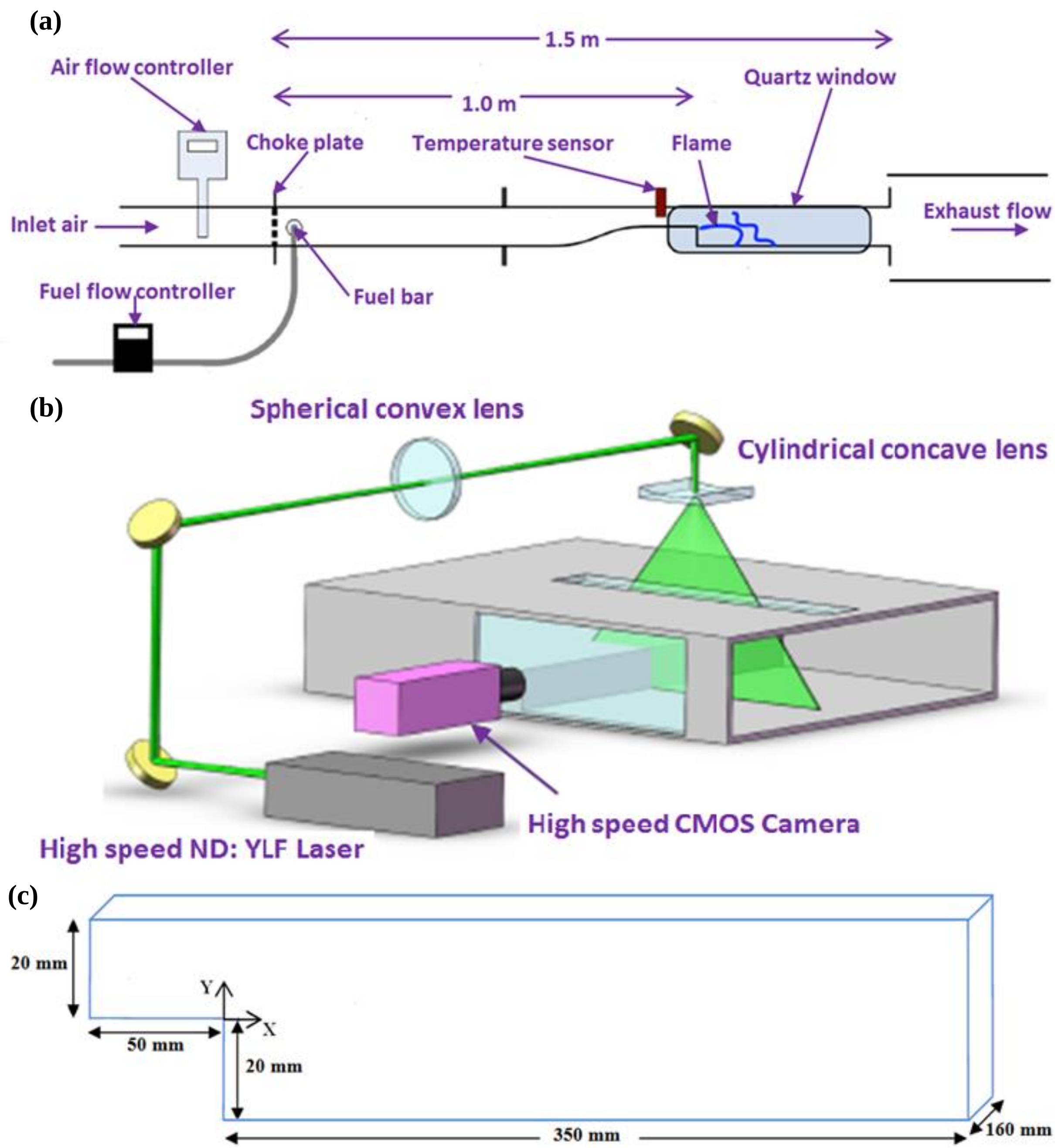

Fig.1 Schematic diagrams showing: (a) the experimental set up of the present backward-facing step combustor, (b) the set up for the high speed particle image velocimetry (*PIV*), and (c) the *3-D* representation of the present combustor to be used in the *OpenFOAM* simulations.

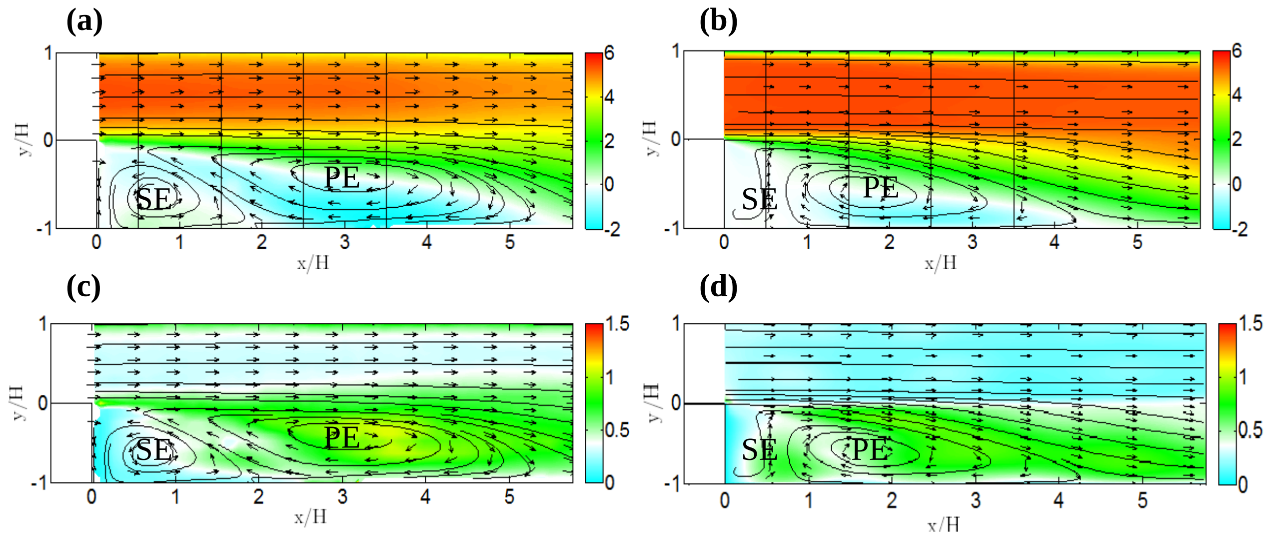

Fig.2 Comparison between the *PIV* data (left) and *LES* model results (right) for the contour plots of average axial velocity (m/s, a and b) and *rms* axial velocity (m/s, c and d) plotted on the streamlines of the mean velocity as a background at Φ=0.63.

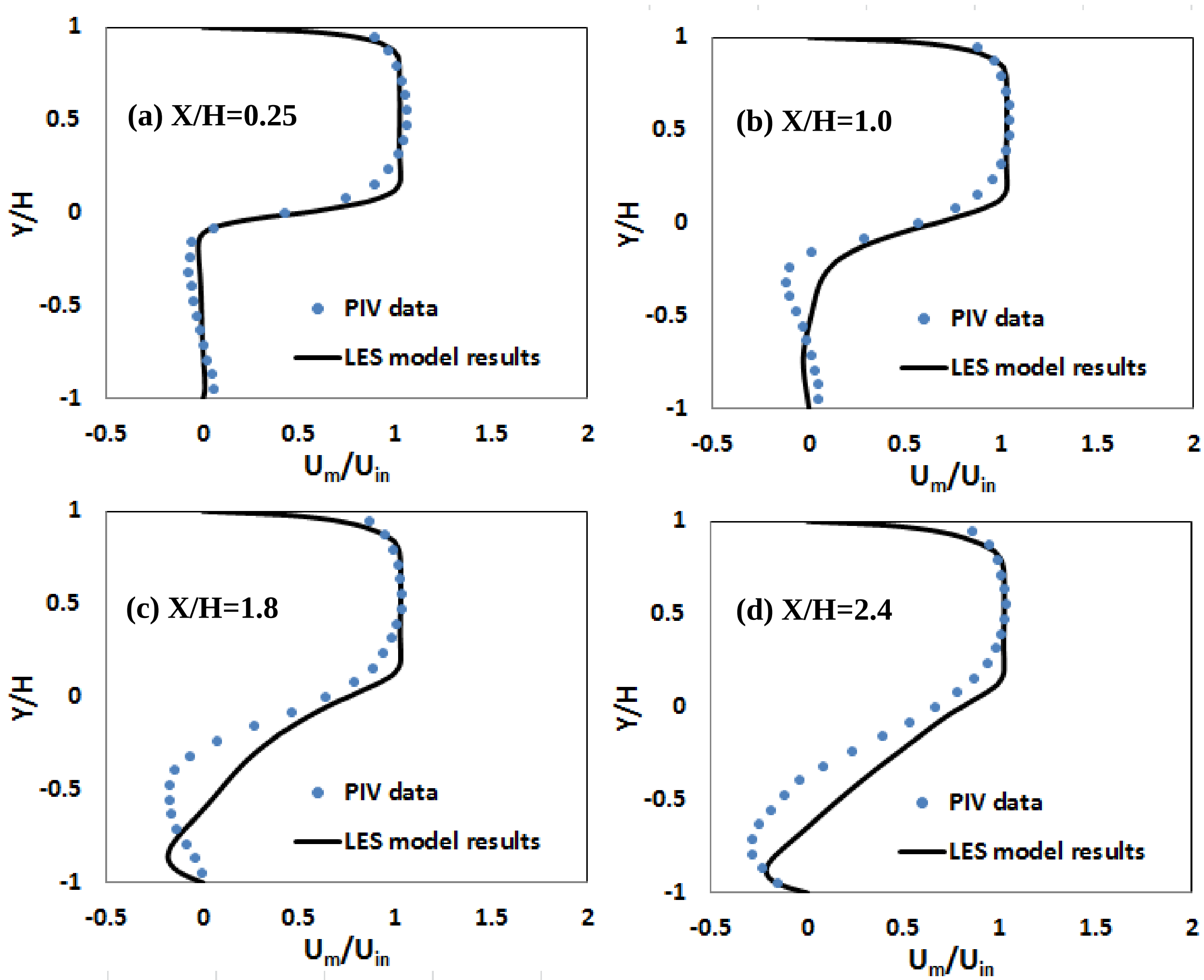

Fig.3 Comparison between the *PIV* data and *LES* model results for the normalized average axial velocity at different normalized axial locations at Φ=0.63.

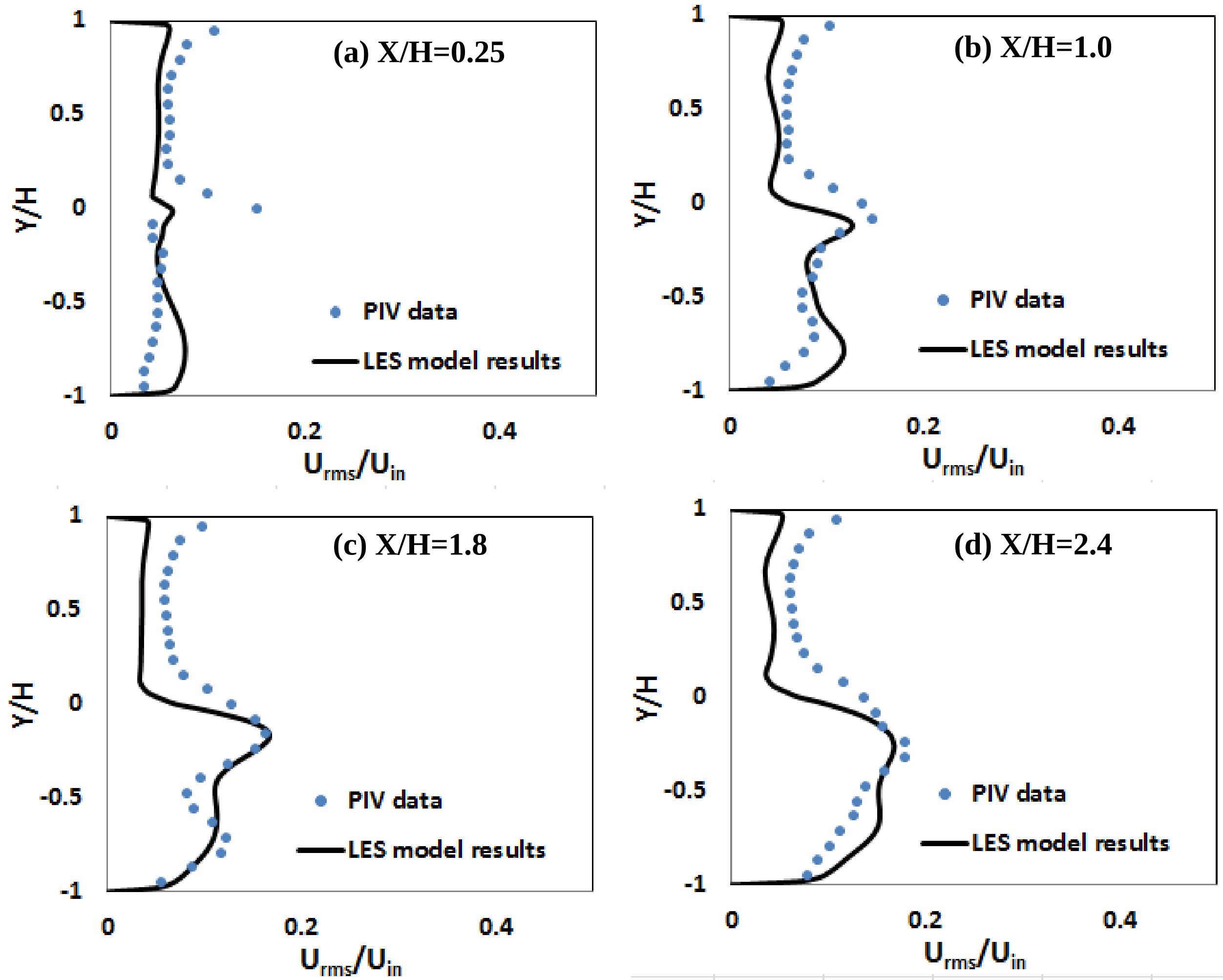

Fig.4 Comparison between the *PIV* data and *LES* model results for the normalized *rms* axial velocity at different normalized axial locations at Φ=0.63.

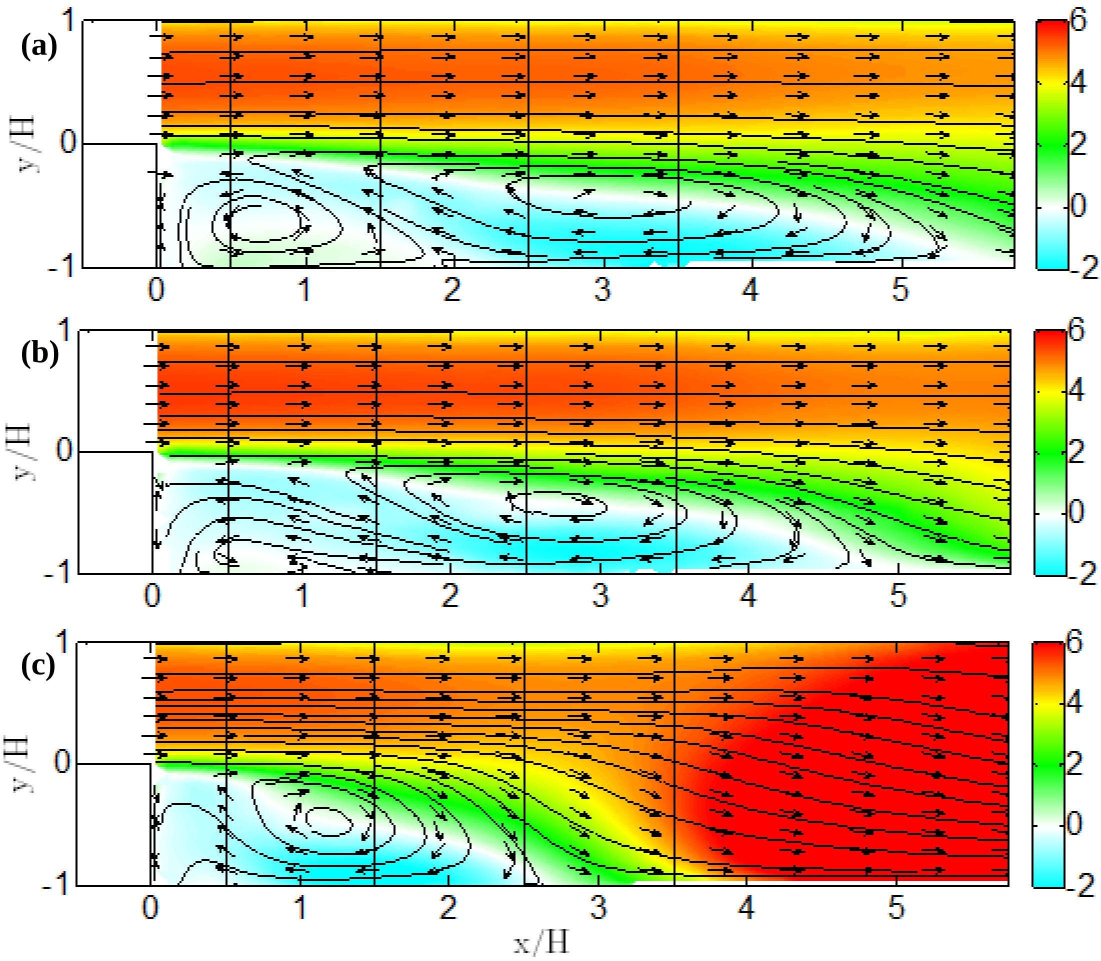

Fig.5 Effect of equivalence ratio on the distribution of the average axial velocity (m/s) based on the *PIV* data: (a) Φ=0.63, (b) Φ=0.69, and (c) Φ=0.85.

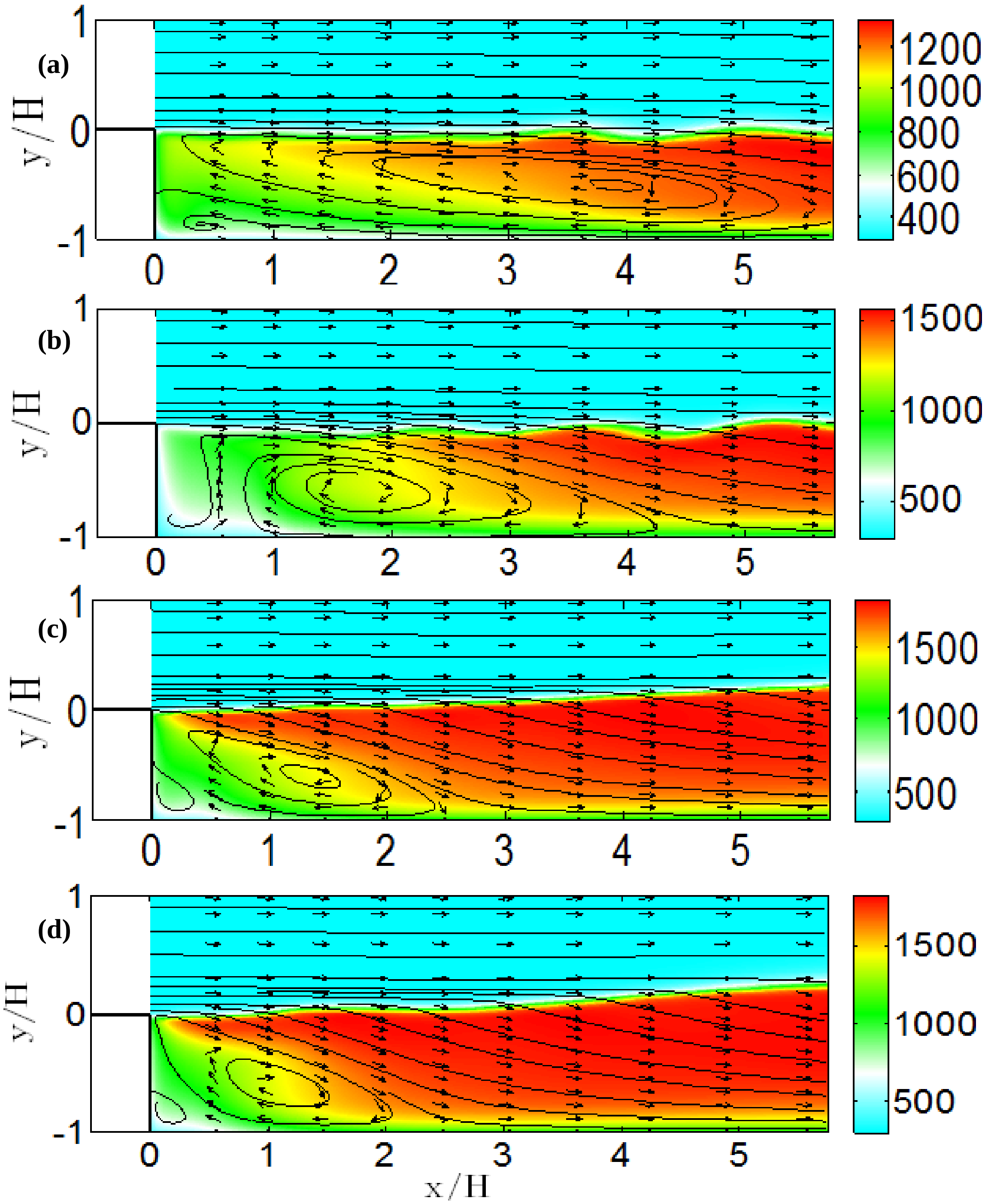

Fig.6 Effect of equivalence ratio on the distribution of the temperature (K) based on the *LES* model results: (a) Φ=0.50, (b) Φ=0.63, (c) Φ=0.75 and (d) Φ=0.85.

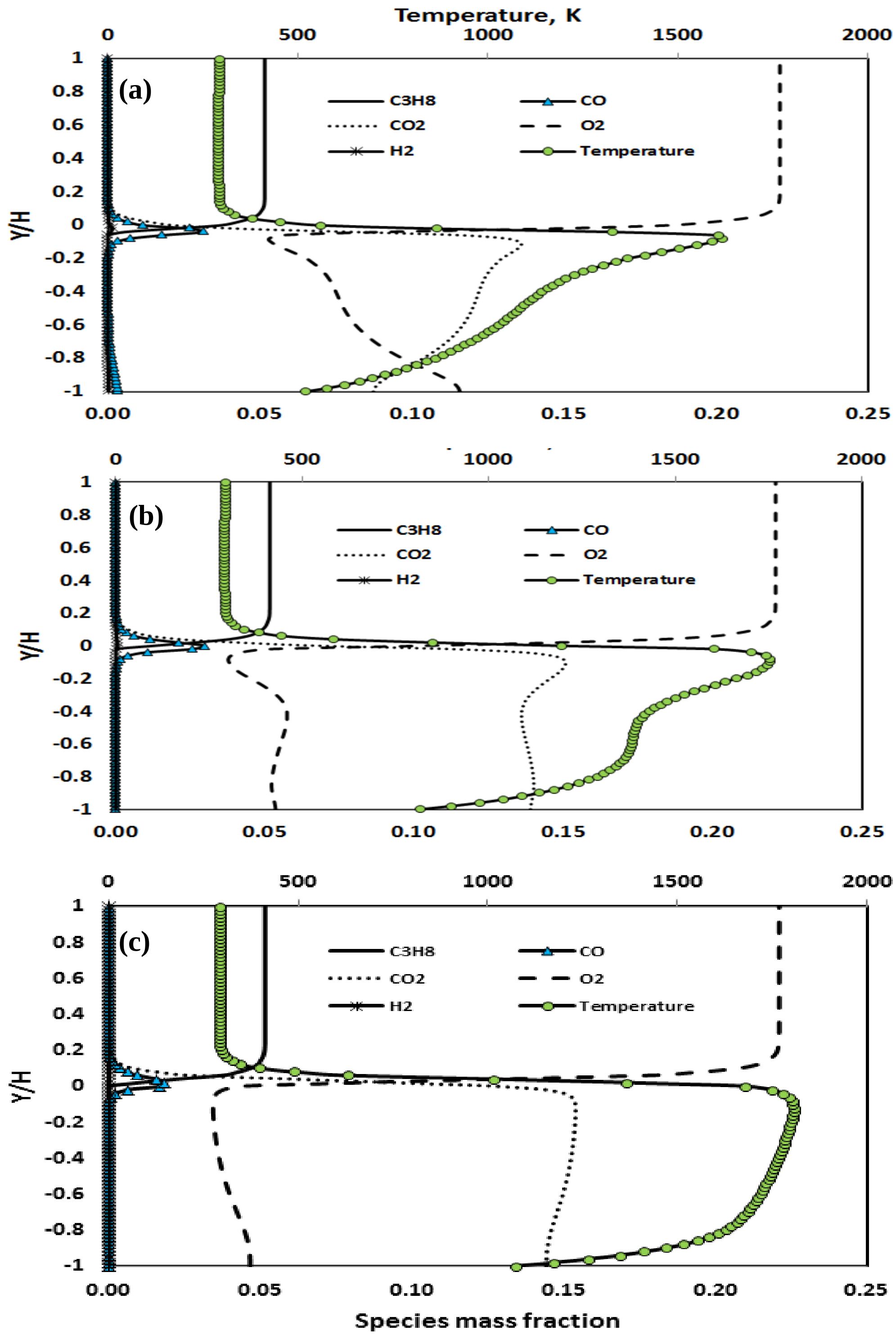

Fig.7 Temperature (K) distributions and species concentrations at different axial locations at Φ=0.85: (a) x/H=0.25, (b) x/H=1.0, and (c) x/H=2.4.

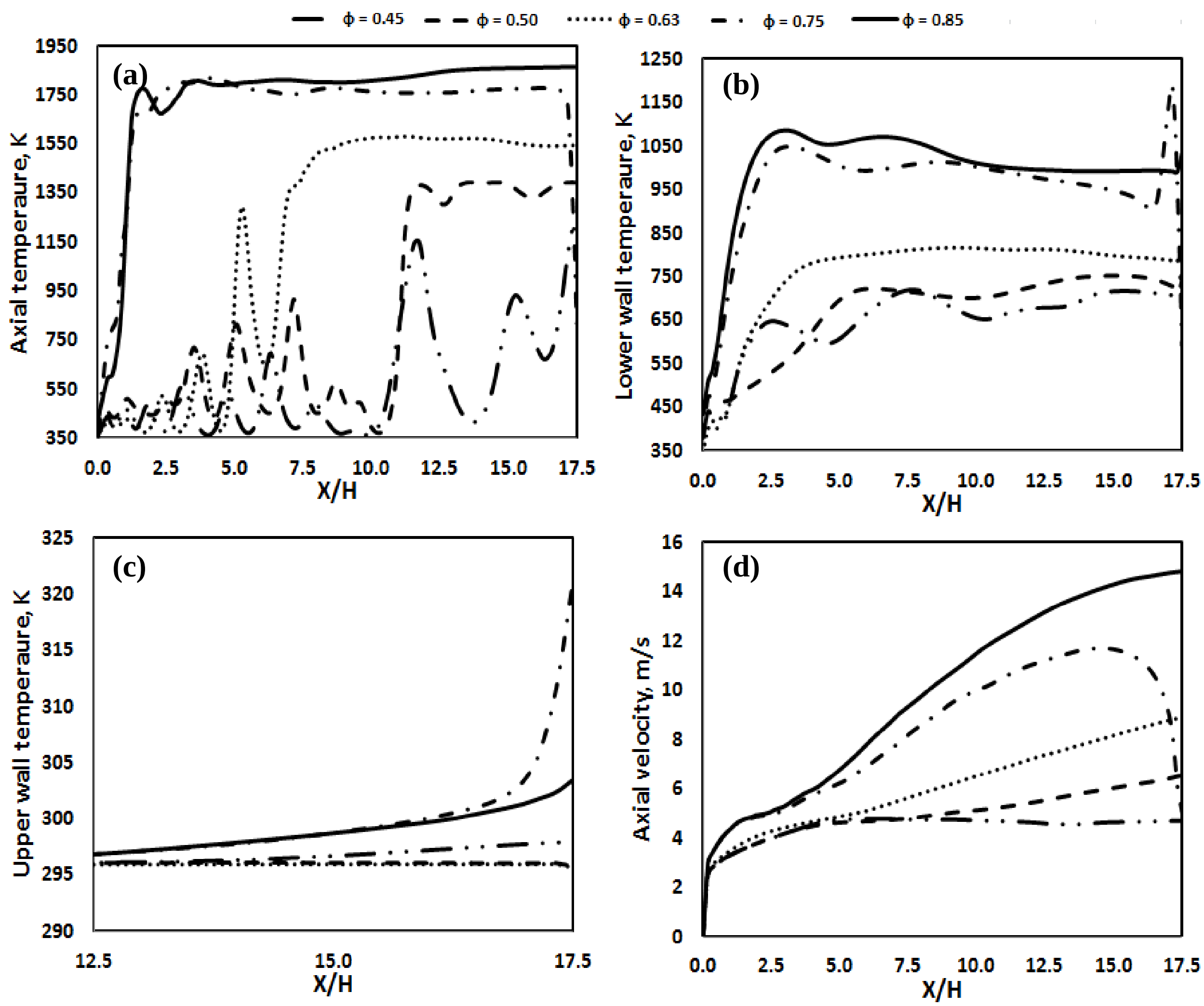

Fig.8 Effect of equivalence ratio on the axial distributions of: (a) temperature (K, through the line *y/H*=0), (b) lower wall temperature (K), (c) upper wall temperature (K), and (d) average axial velocity(m/s, through the line *y/H*=0); based on the *LES* model results.